3-14-2013

Novel Patterns of Torsion-Inversion-Rotation Energy Levels in the ν11 Asymmetric CH-Stretch Spectrum of Methylamine

Mahesh B. Dawadi
The University of Texas Rio Grande Valley, mahesh.dawadi@utrgv.edu

C. Michael Lindsay

Andrei Chirokolava

David S. Perry

Li Hong Xu

The Journal of Chemical Physics

Novel patterns of torsion-inversion-rotation energy levels in the ν_{11} asymmetric CH-stretch spectrum of methylamine

Cite as: J. Chem. Phys. **138**, 104305 (2013); https://doi.org/10.1063/1.4794157
Submitted: 28 November 2012 . Accepted: 20 February 2013 . Published Online: 11 March 2013

Mahesh B. Dawadi, C. Michael Lindsay, Andrei Chirokolava, David S. Perry, and Li-Hong Xu

AIP Publishing

Novel patterns of torsion-inversion-rotation energy levels in the ν_{11} asymmetric CH-stretch spectrum of methylamine

Mahesh B. Dawadi,[1] C. Michael Lindsay,[1,a)] Andrei Chirokolava,[1,b)] David S. Perry,[1,c)] and Li-Hong Xu[2]
[1]*Department of Chemistry, The University of Akron, Akron, Ohio 44325, USA*
[2]*Department of Physics, Centre for Laser, Atomic and Molecular Studies (CLAMS), University of New Brunswick, Saint John, New Brunswick E2L 4L5, Canada*

(Received 28 November 2012; accepted 20 February 2013; published online 11 March 2013)

The high-resolution infrared spectrum of methylamine (CH_3NH_2) has been recorded using slit-jet direct absorption spectroscopy in the ν_{11} CH-stretch region (2965–3005 cm^{-1}) with a resolution of 0.0025 cm^{-1}. The 621 lines assigned by ground state combination differences represent 27 substates with $|K'| \leq 2$ for the A, B, E_1, and E_2 symmetries. The spectrum of CH_3NH_2 is complicated by torsion and inversion tunneling connecting six equivalent minima. The upper states $K' = 0, \pm 1$ for E_1 and E_2 are substantially perturbed by "dark" states. The result in the spectrum is multiplets of 2 or 3 states with mixed bright/dark character. The analysis of the spectrum reveals two qualitative differences in the energy level pattern relative to the vibrational ground state and relative to available data on the lower frequency vibrations (NH_2 wag and CN stretch). First at $J' = 0$, there is a different ordering of the levels connected by torsion-inversion tunneling. Second, the low-J splittings indicative of torsion-rotation coupling are greatly reduced in the ν_{11} excited state relative to the vibrational ground state for both the E_1 and E_2 species, suggesting the partial suppression of torsional tunneling in the ν_{11} CH-stretch excited state. © *2013 American Institute of Physics*. [http://dx.doi.org/10.1063/1.4794157]

I. INTRODUCTION

CH_3NH_2 is a prototypical molecule with two large amplitude degrees of freedom: the internal rotation of the methyl (CH_3) group (ν_{15} torsional motion) and the inversion motion of the hydrogen atoms of the amine (NH_2) group (ν_9 wagging motion).[1–4] The two large amplitude vibrations (LAV) are coupled to each other and to the small amplitude vibrations (SAV).[3–6] These couplings are reflected in the energy level structure and impact the patterns of transitions observed in microwave and infrared spectra.

The potential energy surface for the ground electronic state of methylamine has six equivalent minima connected by torsional and inversion tunneling. The tunneling dynamics can be understood in terms of the torsional and inversion tunneling parameters, $h_{3v} = -0.083$ cm^{-1} and $h_{2v} = -0.052$ cm^{-1}, respectively.[3,7–9] The order of the energy levels in the ground state tunneling multiplet (at $K'' = 0$, $J'' = 0$) is $A_1 < B_1 < E_1 < E_2$.[10] Since the C_S point group designations are not adequate for labeling the resolved tunneling states, these vibrational symmetry species refer to irreducible representations in the G_{12} molecular symmetry group.[11] For $K'' > 0$, the term values show a sinusoidal variation when plotted as K''-reduced energies (Fig. 3 of Ref. 12).

In vibrationally excited states where one of the LAV is excited, a change in the ordering of the levels in the tunneling multiplet is possible. For example, in the ν_9 wagging excited vibration of methylamine, the inversion tunneling parameter increases in magnitude by about 40× to $h_{2v} = -1.93$ cm^{-1}[13] while the torsional tunneling parameter increases more modestly to $h_{3v} = -0.152$ cm^{-1}. The result[13,14] is the tunneling ordering for the wagging excited state: $A_1 < E_1 < E_2 < B_1$. Other examples of LAV excitation producing changes in the ordering of tunneling doublets are the torsionally excited states of S_1 acetaldehyde[15] and the excited wagging state of NH_2D.[16]

In vibrationally excited states where one of the SAV is excited, three kinds of changes in the patterns of the torsion-inversion-rotation energy level structure might be observed. First, quantitative changes in the tunneling spacings and accompanying changes in the periodic torsion-rotation structure variation with K' might be observed while maintaining the "normal" ordering of the torsion-inversion tunneling multiplets. An example of such a case is the CN stretch fundamental band of methylamine[12,17] where both the ordering of the tunneling levels and the pattern of variation with K' are qualitatively the same as in the ground state. The K'-dependent amplitude associated with the inversion splitting is very close to the ground state value, but the amplitude associated with torsional tunneling is increased by 50% indicating a lower effective torsional barrier in the CN stretch excited state.[12] This case can be understood in terms of an approximate adiabatic separation of the LAV from the SAV, in which the motion in the (slow) LAV is considered to occur in an effective potential determined by the (fast) SAV. Thus, the effective torsional or inversion barrier can be different in the SAV vibrationally excited state, resulting in a quantitative change in the tunneling splittings. For example, such an adiabatic treatment of the torsional barrier has been applied to the ν_1 OH and ν_3 symmetric

a)Present address: U.S. Air Force Research Laboratory, 2306 Perimeter Rd., Eglin AFB, Florida 32542, USA.
b)Present address: Bert-Brecht str. 28, 65201 Wiesbaden, Germany.
c)Author to whom correspondence should be addressed. Electronic mail: dperry@uakron.edu.

CH stretch vibrationally excited states of methanol.[18–20] Typically, the same form of the spectroscopic Hamiltonian can be used in this case to fit both ground state and excited state spectra.

The second kind of change that might occur when a SAV is excited is a qualitatively different ordering of the tunneling levels. Until the present work, such a case has not been observed in methylamine. However, in methanol, the asymmetric CH stretches, ν_2 and ν_9,[21–24] and a number of other fundamental bands[24,25] have been found to have inverted torsional tunneling splittings relative to the ground state. Fehrensen *et al.*[19] provided a systematic explanation for the inverted torsional tunneling splittings in methanol by including the concept of geometric phase in their adiabatic treatment and solving for torsional wavefunctions with 4π boundary conditions. This invokes the application of geometric phase in the adiabatic separation of the LAV and SAV. A number of other theoretical approaches have also been applied to the inverted tunneling in methanol.[24–27]

The third kind of change results from "accidental" perturbations by nearly resonant overtone or combination vibrations. Perturbations may shift some of the levels in a tunneling multiplet by larger amounts or in different directions than others. Such "contamination"[28] of the tunneling pattern results in splittings that are not characteristic of an effective barrier in the large amplitude coordinate. In fact, as has been shown for three bands in the fingerprint region (900–1050 cm^{-1}) of propene, the relative perturbation shift may be large enough to change the sign of the tunneling splitting.[28] In general, one finds that perturbations occur in the same spectra as the systematic effects discussed above.[12,13,17]

This paper reports the high-resolution infrared spectrum of the ν_{11} asymmetric CH-stretch band (2965–3005 cm^{-1}) of jet-cooled methylamine, including assignments, a perturbation analysis, and plots of K'-reduced term values. The impact of the asymmetric CH stretch excitation on the torsion-inversion-rotational energy level structure is explored.

II. EXPERIMENTAL

Direct absorption detection under sub-Doppler slit-jet conditions was used to record the high-resolution IR spectrum of methylamine in the ν_{11} CH-stretch region (2965–3005 cm^{-1}). A detailed description of the experimental set-up has been previously reported,[23,29] therefore, only a brief summary will be given here. An F-center laser (Burleigh FCL-10), optically pumped by a Coherent Krypton ion laser, provides single mode, continuous wave, continuously tunable infrared light from 2.3 to 3.3 μm. A pulsed 2 × 0.01 cm slit nozzle and multi-reflection cell[30] were used to increase the infrared absorption optical path length and the resolution. The infrared spectrum is obtained by recording the intensity of transmitted light with an InSb detector as the laser frequency is scanned. A mixture of 10% by volume methylamine in argon was expanded through the slit nozzle at a backing pressure of 100 kPa. Two matched InSb detectors, one before and the other after the slit jet, were used to reduce noise by baseline subtraction.

The residual Doppler width in the slit-jet is 0.0025 cm^{-1}. Relative wavenumber calibration of the recorded lines is achieved with a temperature-controlled sealed 150 MHz marker etalon with a precision of ∼0.00025 cm^{-1} as judged by the standard deviation of combination loops involving a set of more intense infrared lines. Absolute wavenumber calibration is established by a fit of the marker etalon fringe positions to ethylene gas cell absorption lines[29] (standard deviation 0.0005 cm^{-1}).

III. RESULTS AND DISCUSSION

A. Overview of the spectrum

The high resolution infrared spectrum in the ν_{11} asymmetric CH-stretch band is shown in Fig. 1 and the transition wavenumbers along with the relative intensities are tabulated in Table S-I of the supplementary material.[31] The observed spectrum has 1543 lines, and most above 2985 cm^{-1} are assigned. The lower wavenumber part of the spectrum has many unassigned lines, which may belong to the ν_2 asymmetric CH-stretch band and also to perturbing bands.[21] The equally spaced Q-branches clearly evident in Fig. 1 are the signature of $\Delta K = \pm 1$ selection rules in a near-prolate asymmetric rotor. On close inspection, each of these Q-branches is a stack of sub-Q-branches corresponding to the various symmetry species in the G_{12} molecular symmetry group.

B. Symmetry, selection rules, and spectroscopic background

This paper follows the notation of Ohashi and Hougen.[2] The symmetry species in the G_{12} molecular symmetry group are $\{A_1, A_2, B_1, B_2, E_1, \text{and } E_2\}$[2] and are, respectively, equivalent to $\{A_1', A_2', A_2'', A_1'', E'', \text{and } E'\}$.[11] The traditional notation $\{A_s, A_a, E_s, \text{and } E_a\}$ corresponds to $\{A, B, E_1, \text{and } E_2\}$,[12,32] where the 1–2 distinction in the non-degenerate species has been suppressed. The A, B, E_1, and E_2 torsion-wagging-rotation species combine with different nuclear spin combinations that have their respective nuclear spin statistical weights.[2,4,12,32]

In the vibrational ground state, the species of the torsion-wagging-rotation states are ${}^{twr}\Gamma'' = A_1 + B_1 + E_1 + E_2$ for $K'' = 0$, and $A_1 + A_2 + B_1 + B_2 + 2E_1 + 2E_2$ for $K'' \neq 0$.[2] Note that the symmetries of basis functions for the individual degrees of freedom may not be unique in permutation-inversion group theory; however, the species of the observable quantum states, which represent the combined torsion-wagging-rotation motion, are unique. For example, different authors[2,11] employ different species in G_{12} for the rigid rotor basis functions.

Likewise, the symmetries of the vibrational normal modes are not uniquely determined in the presence of large-amplitude motion.[11,33] In the usual spectroscopic convention, the normal modes of methylamine are categorized and numbered in the C_S point group as it applies to the global minimum-energy conformation. The two asymmetric CH stretches are ν_2 and ν_{11}, which are A′ and A″, respectively, in C_S. Of these, the fundamental ν_{11} is higher in frequency[34,35]

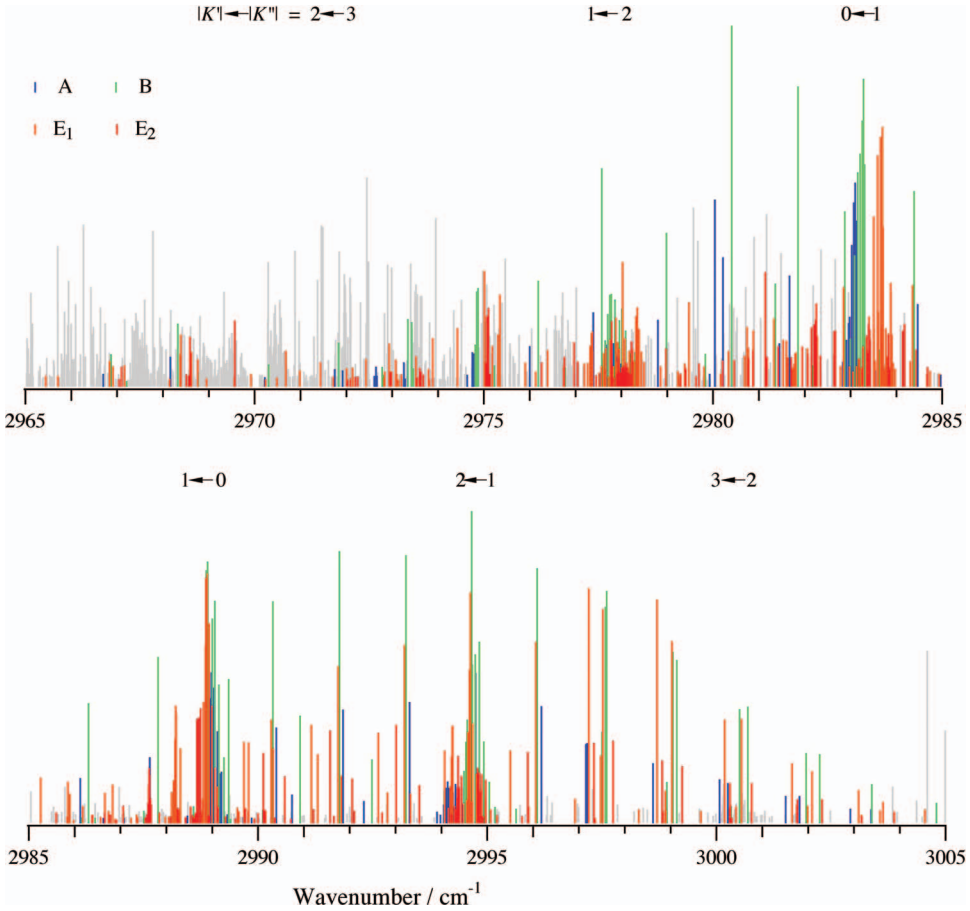

FIG. 1. A stick representation of the slit-jet infrared spectrum of CH_3NH_2 in the ν_{11} CH-stretch region (2965–3005 cm^{-1}), with $|K'| \leftarrow |K''|$ transitions labeled. The assigned transitions for A, B, E_1, and E_2 species are colored with blue, green, orange, and red, respectively. The grey lines indicate all unassigned transitions in the observed spectrum.

and is the subject of this work. In the presence of large-amplitude motion, there are multiple choices for the symmetry species of the normal modes in the G_{12} molecular symmetry group.[11,33] The choices for the pair of asymmetric CH stretches ν_2 and ν_{11} are $A_1 + A_2$, $B_1 + B_2$, E_1, or E_2 (Table 15-4 of Ref. 11). Following Bunker and Jensen's analysis for nitromethane (Eqs. (15)–(65) of Ref. 11), we identify the second choice, B_1 for ν_2 and B_2 for ν_{11}, as the "best" choice for methylamine. Accordingly, the species of the torsion-wagging tunneling multiplet at $J' = 0$ of the ν_{11} vibrationally excited state are ${}^{twrv}\Gamma' = B_2 \otimes \{A_1 + B_1 + E_1 + E_2\} = \{B_2 + A_2 + E_1 + E_2\}$.

CH_3NH_2 is a slightly asymmetric prolate top with an asymmetry parameter ($\kappa = -0.97$). When symmetric top notation is used, we identify $|K| \equiv K_a$. The transition dipole moment of the ν_{11} band is in the direction of the *b*-rotational axis, that is, parallel to a line connecting the two-amine hydrogens. The rigid near-prolate asymmetric rotor rotational selection rules for *b*-type transitions are $\Delta J = 0, \pm 1$ (except $J = 0 \nleftrightarrow J = 0$); $\Delta K_a = \pm 1$; and $\Delta K_c = \pm 1, \pm 3$. In the G_{12} group, allowed transitions in methylamine[11,36] obey ${}^{twrv}\Gamma' \otimes {}^{twrv}\Gamma'' \otimes A_2' \supset A_1$; where ${}^{twrv}\Gamma'$ and ${}^{twrv}\Gamma''$ are the torsion-wagging-rotation-vibration species of methylamine in the excited and ground states, respectively. Thus, $A_1 \leftrightarrow A_2$; $B_1 \leftrightarrow B_2$; $E_1 \leftrightarrow E_1$; $E_2 \leftrightarrow E_2$.[2]

The non-rigidity of methylamine gives rise to further complications in the rotational selection rules.[37] For the ${}^{twrv}\Gamma = A$ and B species, the rotational wave functions are well described as rigid asymmetric rotor functions, and these species obey *b*-type rotational selection rules as above. As usual, the asymmetric rotor Hamiltonian has four blocks according to the Viergruppe symmetries of the Wang functions[36]

$$|JK\gamma\rangle = \frac{1}{\sqrt{2}}(|JK\rangle + (-1)^{\gamma}|J, -K\rangle), \qquad (1)$$

where $\gamma = 0$ or 1 for $K > 0$ and $|JK\gamma\rangle = |JK\rangle$ for $K = 0$. The symmetric rotor functions are notated as $|JK\rangle$ and $|J, -K\rangle$ where the quantum number M has been suppressed. In the present near-prolate asymmetric rotor limit, each rotational wavefunction for the A and B species is well-approximated by one of the Wang functions. For the E_1 and E_2 species, the rotational wavefunctions are linear combinations of the $\gamma = 0$ and 1 Wang functions for a given K, with the result that "extra" rotational transitions appear in the spectrum.[37] In the context of the Wang basis, these "extra" transitions appear to have *c*-type selection rules, but can alternatively be interpreted as *b*-type transitions between states of mixed rotational symmetry. A symmetric rotor-like notation with a signed value of K has been used in the literature for the E species,[1,38] and the levels are labeled E_{1+1} and E_{2+1} for $K \geq 0$, and E_{1-1} and

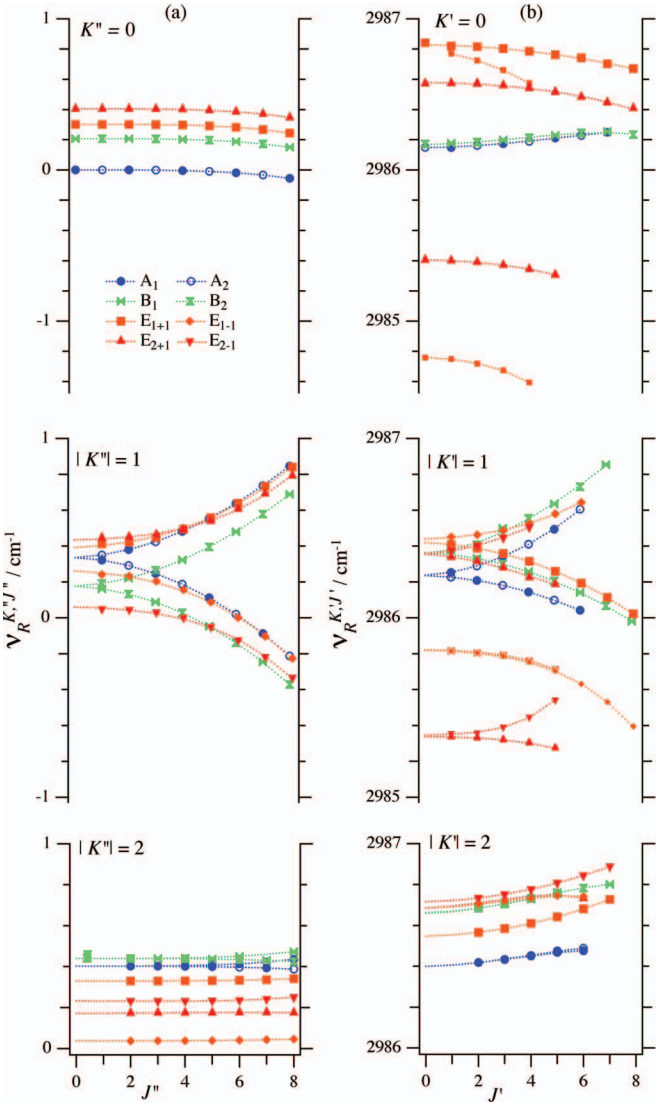

FIG. 2. Reduced term values of the ground (a) and excited (b) vibrational states plotted as a function of angular momentum quantum number (J). The plotted term values are $\nu_R{}^{K,J} = \nu^{K,J} - \frac{1}{2}(B'' + C'')J(J+1) - [A'' - \frac{1}{2}(B'' + C'')]\,K^2$, where the ground state rotational constants are from Refs. 3 and 35. Perturbations in the E_1 and E_2 species result in 2 or 3 upper state levels with the same J', K', Γ' assignment, and their relative intensities are indicated approximately by the area of the markers.

E_{2-1} for $K < 0$. In this symmetric rotor basis, there are "extra" symmetric rotor-forbidden ($\Delta K = \pm 3$) transitions that arise from the mixed rotational character (e.g., $E_{1+1} \leftrightarrow E_{1-1}$) of the $|K| = 1$ levels. Such transitions have been reported in the NH_2 wagging band of methylamine.[13]

For the vibrational ground state of methylamine, the splitting patterns of the rotational levels are shown in Fig. 2(a). For the A and B species, the asymmetry splittings behave as expected[39] for a rigid near-prolate asymmetric rotor, approaching 0 as $J'' \rightarrow 0$. For the E_1 and E_2 species, the $K'' = 1$ splittings approach the rigid asymmetric rotor limit for large J'' (≈7–8), but do not approach 0 as $J'' \rightarrow 0$. The limiting splitting at $J'' = 0$ is a measure of the symmetric rotor torsion-rotation coupling. Thus, these J-dependent splittings might be termed torsion-rotation-asymmetry splittings. These splittings reflect a transition of the $K'' = 1$ rotational wavefunctions from the symmetric rotor limit at low J'' to the asymmetric rotor limit at high J''. At $K'' = 2$, asymmetry in this near-prolate top contributes less to the splittings, and all of the plotted J'' values are close to the symmetric rotor limit.

TABLE I. The numbers of symmetric-rotor allowed ($\Delta K = \pm 1$) and forbidden ($\Delta K = \pm 3$) transitions assigned for E_1 and E_2 species in the methylamine ν_{11} band.

$\lvert K'\rvert \leftarrow \lvert K''\rvert$	$1 \leftarrow 0, 2$		$0, 2 \leftarrow 1$		$2 \leftarrow 3$
${}^{twrv}\Gamma'$	$\Delta K = \pm 1$	$\Delta K = \pm 3$	$\Delta K = \pm 1$	$\Delta K = \pm 3$[a]	$\Delta K = \pm 1$
E_{1-1}	39	8	19	9	6
E_{1+1}	69	10	81	10	6
E_{2-1}	26	8	14	2	6
E_{2+1}	34	10	69	3	2

[a]"Extra" symmetric rotor-forbidden transitions that arise from the mixed ($E_{1+1} \leftrightarrow E_{1-1}$ or $E_{2+1} \leftrightarrow E_{2-1}$) rotational character of the $|K| = 1$ levels.[37]

C. Assignments

The pattern of the torsion-wagging-rotation levels in the vibrational upper state of the ν_{11} CH-stretch fundamental band is not known *a priori*. Coupling of the large amplitude motions to the asymmetric CH-stretch may affect the K-dependent torsion-inversion splittings and also the J-dependent torsion-rotation-asymmetry splittings. Further, accidental perturbations expected for a vibrationally excited state will cause frequency shifts and result in additional observable transitions. Accordingly, in the present work, assignments are based on ground state combination differences[1,38] using the known ground state term values supplied by Ohashi.[35] With the selection rules, $\Delta J = 0, \pm 1$, $\Delta K = \pm 1, \pm 3$, there are up to 12 possible transitions reaching particular J', K', ${}^{twrv}\Gamma'$ upper states, of which a maximum of 8 have been assigned in this work. The only $\Delta K = \pm 3$ transitions observed are those "extra" transitions that are expected from the mixed rotational character of the $|K| = 1$ levels. The precision of ~0.00025 cm^{-1} in these combination loops provides considerable confidence in the assignments.

In total, 621 lines out of 1543 recorded lines were assigned and are tabulated in Tables S-II–S-V of the supplementary material.[31] Table I summarizes the number of symmetric-rotor allowed and forbidden transitions assigned for the degenerate species. The transitions of the E_1 and E_2 species for $K' = 0, +1, -1$ are perturbed (Table II). Because of the challenges posed by numerous perturbations and because of the lack of a torsion-inversion-rotation Hamiltonian suitable for the CH-stretch excited state, a detailed global fit of the observed transitions has not been attempted.

D. Reduced term values

For the purpose of visualizing the trends of the state energies, it is convenient to represent them as reduced term values from which the rigid symmetric rotor part of the energy has been subtracted. The individual rotational levels of the upper and lower vibrational states are thus represented as reduced term values in Fig. 2. Vibrational substates are specified by

TABLE II. Substate origins, reduced substate term values, and effective rotational constants.[a]

Substate identifiers[b]	$\|K'\|$	${}^{twrv}\Gamma'$	$\nu_0^{K'}$ (cm^{-1})	B_{eff} (cm^{-1})	D_{eff} (10^{-6} cm^{-1})	$\nu_R^{K'}$ (cm^{-1})	$\sum I^{K'}$
100	0	A	2986.146(1)	0.7418(2)	10(3)	2986.147	168
200	0	B	2986.168(2)	0.7424(3)	27(4)	2986.168	368
300[c]	0	E_{1+1}	2986.791(2)	0.7282(4)	−18(2)	2986.792	64
301	0	E_{1+1}	2986.827(4)	0.7374(3)	0.89(41)	2986.828	259
302[c]	0	E_{1+1}	2984.758(2)	0.7339(6)	13(2)	2984.758	46
500[c]	0	E_{2+1}	2985.405(1)	0.7368(1)	24(1)	2985.405	97
501[c]	0	E_{2+1}	2986.578(1)	0.7377(3)	96(12)	2986.579	96
110	1	A	2988.928(1)	0.7484(4)	−31(10)	2986.227	89
110	1	A	2988.926(1)	0.7347(1)	2.3(10)	2986.225	123
210	1	B	2989.060(1)	0.7339(1)	0.4(4)	2986.359	320
210	1	B	2989.055(2)	0.7501(20)	25(35)	2986.354	185
310[c]	1	E_{1+1}	2989.121(1)	0.7343(1)	5.4(10)	2986.419	244
311[c]	1	E_{1+1}	2988.521(1)	0.7371(1)	49(1)	2985.819	171
410[c]	1	E_{1-1}	2989.141(2)	0.7433(3)	−24(6)	2986.439	224
411[c]	1	E_{1-1}	2988.523(3)	0.7378(4)	66(11)	2985.821	25
510[c]	1	E_{2+1}	2989.056(5)	0.7324(8)	−46(26)	2986.269	104
511[c]	1	E_{2+1}	2988.038(1)	0.7384(2)	38(4)	2985.337	69
610[c]	1	E_{2-1}	2989.058(3)	0.7472(6)	19(26)	2986.357	57
611[c]	1	E_{2-1}	2988.049(6)	0.7409(10)	−17(1)	2985.347	22
120	2	A	2997.204(2)	0.7427(3)	33(5)	2986.399	70
120	2	A	2997.204(3)	0.7428(4)	28(7)	2986.399	37
220	2	B	2997.464(2)	0.7438(2)	20(3)	2986.658	134
220	2	B	2997.468(1)	0.7432(1)	32(4)	2986.663	137
320	2	E_{1+1}	2997.352(1)	0.7425(1)	−0.27(7)	2986.547	146
420	2	E_{1-1}	2997.489(3)	0.7429(3)	49(5)	2986.684	146
520	2	E_{2+1}	2997.490(9)	0.7440(9)	80(21)	2986.685	53
620	2	E_{2-1}	2997.521(1)	0.7425(1)	−0.94(14)	2986.716	63

[a]Substate origins ($\nu_0^{K'}$) and reduced substate term values ($\nu_R^{K'}$) are related by Eq. (3). For $\nu_0^{K'}$, B_{eff}, and D_{eff} the uncertainties are given as two standard deviations of the fit (in parentheses) in units of last digit. $\sum I^{K'}$ is the sum of the intensities for each substate.

[b]The substate identifiers are used in the detailed line lists in the supplementary material. The first digit of substate identifier encodes the symmetry, ${}^{twrv}\Gamma'$, the second digit is K', and the last digit distinguishes the levels in an interaction doublet or triplet. The deperturbation results for these multiplets are summarized in Table III.

[c]Perturbed substates for E_1 and E_2 species with $K' = 0, +1, -1$.

the combination of the K rotational quantum number and the symmetry species. The computation of reduced substate term values is explained in the next paragraph.

The upper state term values ($\nu^{K',J'}$) of the ν_{11} CH-stretch are obtained by adding the relevant ground state term values to the wavenumber of each observed transition. Then the upper state term values were fit to the expression:

$$\nu^{K',J'} = \nu_0^{K'} + B_{eff}^{K'} J'(J'+1) - D_{eff}^{K'} J'(J'+1)^2, \qquad (2)$$

where B_{eff} and D_{eff} are effective rotational and effective centrifugal distortion constants, respectively. The resulting substate origins $\nu_0^{K'}$ are converted to reduced substate term values $\nu_R^{K'}$ by subtracting the remaining symmetric-rigid-rotor energy,

$$\nu_R^{K'} = \nu_0^{K'} - \left[A'' - \frac{(B''+C'')}{2}\right] K'^2. \qquad (3)$$

The excited substate origins ($\nu_0^{K'}$) and reduced term values ($\nu_R^{K'}$) are listed in Table II.

E. Perturbation analysis

The ν_{11} fundamental of CH_3NH_2 exhibits multiple perturbations affecting most of the E_1 and E_2 upper state rotational levels. Each perturbation reflects the mixing of a "bright" rotational level[40] of the ν_{11} vibrationally excited state with rotational levels of one or more nearly resonant "dark" vibrational states. In the deperturbation analysis below, it is assumed that the rotational levels of the dark vibrational states carry no oscillator strength from the ground state. When a perturbation mixing occurs, the "dark" rotational levels appear as observable transitions in the spectrum with intensities proportional to their "borrowed" bright state character. The extent of mixing depends on the size of the coupling matrix elements relative to the zeroth-order energy spacings.

The signature of these perturbations is the fragmentation of expected single lines into a multiplets of two or three transitions with the same J', K', Γ' assignment (Fig. 2(b) and Table II). Such perturbations were not found for the A and B species. It is likely that there are additional perturbations in the present spectrum—for the A and B species as well as for the E_1 and E_2 species—for which the relevant "dark" levels did not borrow sufficient intensity to be detected at the present sensitivity and resolution. Such additional undetected perturbations may still cause frequency shifts of the observed transitions. The evident propensity for more perturbations in the degenerate E_1 and E_2 species could be attributable in part to the expected larger numbers of the degenerate vibrational states among the nearly resonant "dark" combination and overtone vibrations.[41]

To determine the hypothetical unperturbed torsion-wagging-rotation tunneling patterns in the vibrationally excited state, it is necessary to deperturb the substates where perturbations occur. In most cases, only a pair of levels is observed, the bright level and one dark level that borrows intensity, and the standard 2-level deperturbation formulae[23,29] may be used. For each interacting pair, the relative intensities as well as the observed transition wavenumbers are needed to determine the hypothetical unperturbed upper state term values $\nu^{J',K'}$ and the effective coupling matrix element, $W_{ij}^{J',K'}$. For one substate, $K' = 0$ E_1, three interacting levels are observed, one bright level and two dark levels, which can be deperturbed using the Lawrance and Knight (LK) method.[42,43] For the case of three interacting levels, there are three possible coupling matrix elements, one connecting each pair. The LK deconvolution yields two matrix elements, the two that connect the bright level to the interacting pair of dark levels. It also yields the deperturbed bright level term value and the term values of the two interacting dark levels. The LK method does not directly give any information about the matrix element coupling the two dark levels to each other, nor does it deperturb the interacting dark levels.

Examples of the derived coupling matrix elements W_{ij} are shown in Fig. 3. For the three interacting levels of the $K' = 0$ E_1 species, two matrix elements are derived at each J', one larger $\sim$0.8 cm^{-1} and one smaller $<$0.2 cm^{-1} (Fig. 3(a)). The larger matrix element shows some scatter, but is approximately independent of J', which is the behavior expected for either anharmonic coupling or for a-axis Coriolis coupling. Since a-axis Coriolis coupling is null for $K' = 0$, it is likely that this matrix element represents anharmonic coupling with the rotational levels of a dark vibrational state. The smaller matrix element increases approximately linearly with $[J'(J' + 1)]^{1/2}$, which is the behavior expected for a *b*- or *c*-type Coriolis interaction.[44] As noted above, we do not know the matrix element and coupling type connecting the two dark states. Given that the two computed matrix elements scale differently with J', one explanation is that the bright level couples to the two dark levels by the indicated mechanisms and the coupling between the dark levels is negligible. Other coupling schemes may also be consistent with the data.

For the $K' = 0$ E_2 species (Fig. 3(b)), there are two interacting levels, one bright and one dark. The deperturbed coupling matrix element is independent of J' at $\sim$0.6 cm^{-1}, indicating anharmonic coupling. The transitions in the E_{1+1}, E_{1-1}, E_{2+1}, and E_{2-1} substates are also perturbed by apparent anharmonic interactions (Fig. S-I of the supplementary material).[31]

The scatter in Fig. 3 arises primarily from uncertainties in the intensity measurements, the wavenumber measurements being much more precise. In addition, these uncertainties result in significant uncertainties in the deperturbed term values. The effect of intensity uncertainties is most readily seen in sets of transitions reaching the same upper state J', K' level via different selection rules, e.g., P, Q, R transitions. Such P, Q, R transitions were deperturbed separately and are represented by separate points in Fig. 3. Since there are multiple determinations of each coupling matrix element, more precise matrix elements can be obtained as the average $\overline{W_{ij}}$ of all independent determinations. In addition to the separate analysis of the P, Q, and R transitions, the J'-dependence (Fig. 3) provides more determinations. Of course, use of the J'-dependent data for this purpose, assumes the validity of the above explanations of the perturbations as one case of *b*/*c*-Coriolis coupling and several cases of anharmonic coupling. Then with the more precise $\overline{W_{ij}}$, more precise deperturbed substate origins can also be calculated. The results of the deperturbation analysis are summarized in Table III. The uncertainties given in Table III and Fig. 4 for the deperturbed term values include only the statistical uncertainties of this analysis. Additional systematic errors likely result from the existence of additional—as yet undetected—perturbing vibrations.

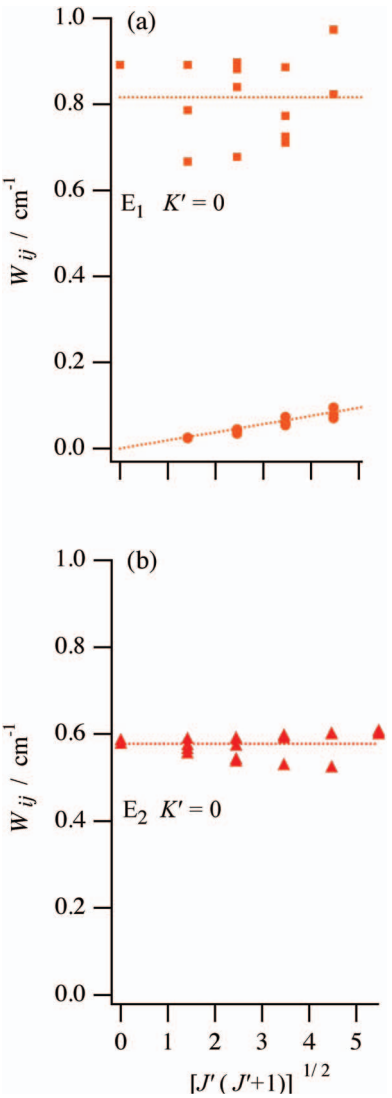

FIG. 3. (a) Coupling matrix elements (W_{ij}) for the $K' = 0$ E_1 species in the excited state as a function of $[J'(J' + 1)]^{1/2}$.[44] Matrix elements attributed to a *b*/*c*-type Coriolis interaction are denoted with circular markers and those attributable to an anharmonic interaction of the same CH-stretch bright states are represented with square markers. (b) Coupling matrix elements W_{ij} attributed to an anharmonic interaction for the $K' = 0$ E_2 species. The lines are fits to the data given the deduced mechanisms: constant with J' for anharmonic and proportional to $[J'(J' + 1)]^{1/2}$ for *b*/*c*-type Coriolis coupling.

TABLE III. Average coupling matrix elements, deperturbed reduced term values, and types of interactions.[a]

$^{twrv}\Gamma'$	K'	$\nu_{dep,R}{}^{K'}$ (cm^{-1})	$\overline{W_{ij}}$ (cm^{-1})	Coupling type
E_{1+1}	0	2986.437(76)	0.82(7)	Anharmonic
E_{1+1}	0		0.018(3) [b]	*b*/*c*-Coriolis
E_{2+1}	0	2986.086(20)	0.58(2)	Anharmonic
E_{1+1}	1	2986.256(21)	0.28(2)	Anharmonic
E_{1-1}	1	2986.322(50)	0.32(5)	Anharmonic
E_{2+1}	1	2986.030(39)	0.42(4)	Anharmonic
E_{2-1}	1	2986.094(50)	0.47(5)	Anharmonic

[a]For average coupling matrix elements $\overline{W_{ij}}$ and upper state deperturbed reduced term values ($\nu_{dep,R}{}^{K'}$), the statistical uncertainties are given as two standard deviations (in parentheses) in units of the last digit. Deperturbed upper state term values $\nu_{dep}{}^{K',J',\Gamma'}$ were calculated from the average matrix elements, fitted to Eq. (2), and reduced according to Eq. (3) using the ground state rotational constants, $A'' - (B'' + C'')/2 = 2.701$ cm^{-1} from Refs. 3 and 35.

[b]For the *b*/*c*-Coriolis interactions (bottom of Fig. 3(a)), the J'-dependent matrix elements were fit to the expression, $W_{ij}^{J'} = \overline{W_{ij}}\ [J'(J'+1)]^{1/2}$.

F. The torsion-inversion-rotation structure

As noted in Sec. III B above and shown in Fig. 2(a), the J''-dependent splittings for the $K'' = 1$ E_1 and E_2 species are predominantly asymmetry splittings at high J'' but become torsion-rotation splittings at low J''. The low-J'' limits of these torsion-rotation splittings are 0.13 and 0.38 cm^{-1} for E_1 and E_2, respectively. Figure 2(b) shows that the pattern is qualitatively different in the vibrationally excited state. In the $|K'| = 1$ E_2 the upper state, a perturbation results in two mixed substates with comparable amounts of bright/dark character, one near 2985.3 cm^{-1} in Fig. 2(b) and the other near 2986.3 cm^{-1}. For each of these substates, one can see in Fig. 2(b) that the torsion-rotation-asymmetry splittings separating the E_{2+1} and E_{2-1} levels approach 0 as $J' \to 0$. The $|K'| = 1$ E_1 upper state behaves similarly, except that the E_1 substate centered near 2986.43 cm^{-1} has a small residual splitting (0.02 cm^{-1}) at $J' = 0$. Thus the $|K'| = 1$ E_1 and E_2 species show little or no torsion-rotation coupling and revert to the rigid asymmetric rotor pattern such as is seen (Fig. 2) for the A and B species in both the ground and excited vibrational states. At $|K| = 2$, the torsion-inversion-rotation splitting patterns for the ground and excited states are more similar. The E_1 and E_2 splittings for $|K'| = 2$ in the upper state are approximately constant showing little variation with J', but the magnitude of the splittings is less than in the ground state.

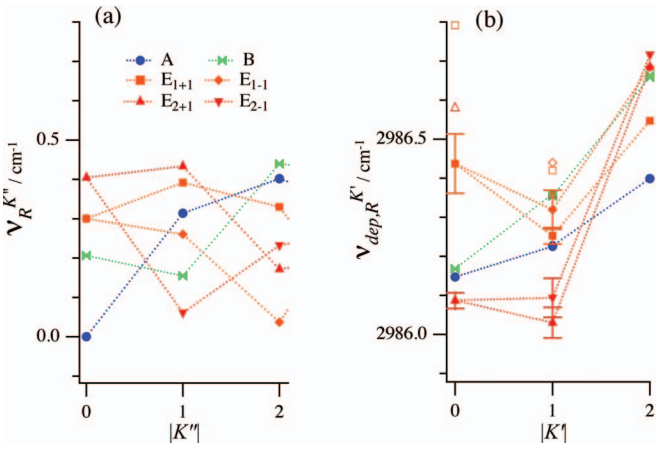

FIG. 4. (a) Reduced substate term values ($\nu_R^{K'}$) for the ground state as a function of rotational quantum number K'' and (b) deperturbed reduced term values ($\nu_{dep,R}{}^{K'}$) as a function of K' for the ν_{11} vibrationally excited state. For the excited state, hollow markers indicate split upper state reduced term values (Table II) while the solid filled markers indicate deperturbed reduced term values for the E_1 and E_2 species (Table III). The error bars, given as two standard deviations, represent the precision of the deperturbation analysis.

Reduced, deperturbed term values, $\nu_{dep,R}{}^{K'}$, for the upper state are compared in Fig. 4 to the corresponding reduced term values, $\nu_R^{K'}$, for the ground state. The ground state torsion-inversion tunneling splittings for methylamine follow the well-established pattern,[3,10,12,38] with the A and B species for $K'' = 0$ at lower energy than the E_1 and E_2 species (Fig. 4(a)). For $|K''| > 0$, the energies of the E_1 and E_2 species split by the torsion-rotation interaction according to the relative signs of the torsional and rotational angular momentum. For example, at $|K''| = 1$, the E_{1+1} states are above the E_{1-1} states and the E_{2+1} states are above the E_{2-1} states (Fig. 4(a)). The K''-dependence of the ground state term values follows a sinusoidal variation (Fig. 3 of Ref. 12) that is most readily appreciated when plotted in terms of Dennison's torsional symmetry index, τ.[12,45] Similar, but simpler, oscillatory patterns are well known in torsional molecules like methanol.[23,46,47] The presence of inversion tunneling in addition to torsional tunneling in methylamine serves to increase the number of symmetry species and to make a more complicated pattern.

The pattern of the torsion-inversion tunneling splittings in the ν_{11} CH-stretch excited state (Fig. 4(b)) is qualitatively different from the ground state. For $K' = 0$, the origin for the E_2 tunneling state is at the bottom of the multiplet, below E_1, A and B, rather than at the top as in the ground state. As noted in the Introduction, the inversion of the ordering of the torsional tunneling states in methanol[21–27] was found to reflect the systematic coupling of the large-amplitude torsional motion to the other SAV, including the asymmetric CH stretches. Since methylamine has analogous torsional tunneling it is not surprising to see the same kind of effect here.

The group theoretical formalism of Hougen and Ohashi[2] allows for a range of tunneling patterns expected in G_{12} molecules. The relative energies of the symmetry species at $J = 0$, $K = 0$ are given[2,48] in terms of the tunneling parameters h_{2v} and h_{3v}:

$$\begin{aligned} E\left({}^{tw}A_1\right) &= +2h_{2v} + 2h_{3v}, \\ E\left({}^{tw}E_1\right) &= +h_{2v} - h_{3v}, \\ E\left({}^{tw}E_2\right) &= -h_{2v} - h_{3v}, \\ E\left({}^{tw}B_1\right) &= -2h_{2v} + 2h_{3v}. \end{aligned} \tag{4}$$

For the ground state of methylamine, the tunneling parameters are both negative, $h_{2v} = -0.052$ and $h_{3v} = -0.083$ cm^{-1}.[3,7,9] In vibrationally excited states, the effective tunneling parameters might have the same signs as for CN stretch[17] or a different sign combination might apply. For example, in the first torsionally excited state of methylamine, which has the "inverted" energy ordering $E_2 < E_1 < B_1 < A_1$, both effective tunneling parameters are positive, $h_{2v} = +0.172$ and $h_{3v} = +2.006$ cm^{-1}.[35] Equation (4), taken in the limit

$h_{2v} \rightarrow 0$, can also be used to model the vibrationally excited states of methanol. For example, the "normal" symmetric CH stretch ν_3[47] can be modeled with $h_{3v} = -3.03$ cm^{-1}, and the "inverted" asymmetric CH stretches, ν_2 and ν_9,[23,24] can be modeled with $h_{3v} = +1.09$ and $+1.83$ cm^{-1}, respectively. Accordingly, one might expect to find a combination of tunneling parameters that accounts for the experimental $K' = 0$ pattern in Fig. 4(b) for the methylamine ν_{11} vibrationally excited state. Unfortunately, the experimental energy ordering, $E_2 < A < B < E_1$, is not consistent with Eq. (4) for any combination of parameters. As noted above, Eq. (4) does allow E_2 to be at the bottom of the tunneling multiplet for a suitable sign combination of h_{2v} and h_{3v}, but not at the same time as E_1 is at the top.

The most likely explanation for the inconsistency of the deperturbed $K' = 0$ term values with Eq. (4) is the presence of additional undetected perturbations that have shifted one or more of the substates enough to change the energy ordering. Whereas in methanol the tunneling splittings are rather large ($\leq$9.1 cm^{-1}), in methylamine the splittings are much smaller ($\leq$0.4 cm^{-1}) and are comparable to the shifts expected from perturbations.

At $|K'| = 1$, the splittings (Fig. 4) between the pair E_{1+1} and E_{1-1}, and between E_{2+1} and E_{2-1} are greatly reduced in magnitude (by 2× and by 6×, respectively) in the excited state relative to the ground state. The $|K'| = 1$ splittings obtained from the deperturbation are actually inverted relative to the corresponding ground states (Fig. 4), but the error bars overlap, meaning that the splittings are small enough that they could be zero within the uncertainties of the deperturbations. For $|K'| = 2$, the splitting between E_{1+1} and E_{1-1} and between the E_{2+1} and E_{2-1} is reduced by about a factor of two relative to the ground state. At $|K'| = 2$, the sign of the E_1 splitting is inverted relative to the ground state while the sign of the E_2 splitting remains the same as in the ground state.

The observation of reduced E_1 and E_2 splittings for $|K'| > 0$ indicates that the torsion-rotation coupling is partially quenched in the ν_{11} CH-stretch excited state of methylamine, which, in turn, suggests a partial suppression of the torsional tunneling in the excited state. Such a suppression of the torsional tunneling splittings has been reported in methanol in the CH stretch overtone region.[25] As noted in the Introduction, the tunneling splittings in the $v_{CH} = 1$ vibrations of methanol can be treated with an adiabatic model in which the (fast) CH stretch motion is solved at each torsional angle and then the (slow) torsional motion is solved in the effective potential that results from the CH stretch excited states. In such an adiabatic model, the character of the fast wavefunctions changes qualitatively along the slow coordinate. For example, in the asymmetric stretch $v_{CH} = 1$ vibrations, the CH amplitude moves between methanol's three CH bonds as the torsional angle changes (Fig. 8 of Ref. 49). At $v_{CH} = 4$ and higher, the spectroscopically accessible CH stretch vibrations in methanol become largely localized in single CH bonds, which means that, in the adiabatic model, 4 or more quanta of CH stretch need to move from one CH bond to the next as the torsional angle changes. Thus in the higher CH stretch overtones, the coupling between localized diabatic states becomes successively higher in order, and therefore, weaker until the adiabatic approximation breaks down and the torsional tunneling is quenched (Fig. 7(a) of Ref. 49). In methylamine, the torsional tunneling rate in the ground state is 36 times slower than in methanol, which means at the $v_{CH} = 1$ level, the coupling between diabatic states is correspondingly weaker than in methanol. The torsional tunneling in methylamine appears to be already somewhat suppressed at the $v_{CH} = 1$ level.

IV. SUMMARY

The high resolution infrared spectrum of the methylamine ν_{11} CH stretch fundamental band reveals different spectral patterns from those in the vibrational ground state, including (i) an altered ordering of the torsion-inversion tunneling levels and (ii) substantially reduced torsion-rotation couplings suggestive of a partial suppression of torsional tunneling in the vibrationally excited state. It is likely that these changes result in part from the systematic coupling of the LAV to the CH stretches and in part from accidental perturbations that have not been fully deperturbed.

ACKNOWLEDGMENTS

The authors are grateful to Xiaoliang Wang and Thomas J. Cronin for their contributions to the experimental work, to Nobukimi Ohashi for helpful discussion and for providing the ground state term values. Support for this work was provided by the Division of Chemical Sciences, Offices of Basic Energy Sciences, Office of Energy Research, and U.S. Department of Energy under Grant No. DE-FG02-90ER14151. L.-H.X. acknowledges financial support for this research from the Natural Sciences and Engineering Research Council of Canada.

[1] U. Merker, H. K. Srivastava, A. Callegari, K. K. Lehmann, and G. Scoles, Phys. Chem. Chem. Phys. **1**, 2427 (1999).
[2] N. Ohashi and J. T. Hougen, J. Mol. Spectrosc. **121**, 474 (1987).
[3] N. Ohashi, K. Takagi, J. T. Hougen, W. B. Olson, and W. J. Lafferty, J. Mol. Spectrosc. **126**, 443 (1987).
[4] L. Sztraka, S. Alanko, and M. Koivusaari, Acta Chim. Hung **130**, 887 (1993).
[5] M. Oda, N. Ohashi, and J. T. Hougen, J. Mol. Spectrosc. **142**, 57 (1990).
[6] N. Ohashi and Y. Toriyama, J. Mol. Spectrosc. **165**, 265 (1994).
[7] V. V. Iyushin, E. A. Alekseev, S. F. Dyubko, R. A. Motiyenko, and J. T. Hougen, J. Mol. Spectrosc. **229**, 170 (2005).
[8] M. Kreglewski and G. Wlodarczak, J. Mol. Spectrosc. **156**, 383 (1992).
[9] V. Ilyushin and F. J. Lovas, J. Phys. Chem. Ref. Data **36**, 1141 (2007).
[10] V. V. Ilyushin, E. A. Alekseev, Y.-C. Chou, Y.-C. Hsu, J. T. Hougen, F. J. Lovas, and L. B. Picraux, J. Mol. Spectrosc. **251**, 56 (2008).
[11] P. R. Bunker and P. Jensen, *Molecular Symmetry and Spectroscopy*, 2nd ed. (NRC Research Press, Ottawa, 1998).
[12] R. M. Lees, Z.-D. Sun, and B. E. Billinghurst, J. Chem. Phys. **135**, 104306 (2011).
[13] I. Gulaczyk, W. Lodyga, M. Kreglewski, and V.-M. Horneman, Mol. Phys. **108**, 2389 (2010).
[14] L. Sztraka, S. Alanko, and M. Koivusaari, J. Mol. Struct. **410–411**, 391 (1997).
[15] Y.-C. Chou, I. C. Chen, and J. T. Hougen, J. Chem. Phys. **120**, 2255 (2004).
[16] M. Halonen and L. Halonen, J. Phys. Chem. A. **110**, 7554 (2006).
[17] I. Gulaczyk, M. Kreglewski, and V.-M. Horneman, J. Mol. Spectrosc. **270**, 70 (2011).
[18] T. N. Clasp and D. S. Perry, J. Chem. Phys. **125**, 104313 (2006).
[19] B. Fehrensen, D. Luckhaus, M. Quack, M. Willeke, and T. R. Rizzo, J. Chem. Phys. **119**, 5534 (2003).

[20]O. V. Boyarkin, T. R. Rizzo, and D. S. Perry, J. Chem. Phys. **110**, 11359 (1999).
[21]S. Twagirayezu, D. S. Perry, J. L. Neill, and M. T. Muckle, J. Mol. Spectrosc. **262**, 65 (2010).
[22]S. Twagirayezu, X. Wang, D. S. Perry, J. L. Neill, M. T. Muckle, B. H. Pate, and L.-H. Xu, J. Phys. Chem. A **115**, 9748 (2011).
[23]L.-H. Xu, X. Wang, T. J. Cronin, D. S. Perry, G. T. Fraser, and A. S. Pine, J. Mol. Spectrosc. **185**, 158 (1997).
[24]X. Wang and D. S. Perry, J. Chem. Phys. **109**, 10795 (1998).
[25]D. S. Perry, J. Phys. Chem. A **112**, 215 (2008).
[26]J. T. Hougen, J. Mol. Spectrosc. **207**, 60 (2001).
[27]J. Castillo-Chara and E. L. Sibert III, J. Chem. Phys. **119**, 11671 (2003).
[28]A. Ainetschian, G. T. Fraser, J. Ortigoso, and B. H. Pate, J. Chem. Phys. **100**, 729 (1994).
[29]A. Chirokolava, D. S. Perry, and L.-H. Xu, J. Mol. Spectrosc. **203**, 320 (2000).
[30]D. Kaur, A. M. De Souza, J. Wanna, S. A. Hammad, L. Mercorelli, and D. S. Perry, Appl. Opt. **29**, 119 (1990).
[31]See supplementary material at http://dx.doi.org/10.1063/1.4794157 for line lists (Tables S-I to S-VI) and details of the deperturbation analysis (Fig. S-I).
[32]M. S. Malghani, R. M. Lees, and J. W. C. Johns, Int. J. Infrared Millimeter Waves **8**, 803 (1987).
[33]J. T. Hougen, J. Mol. Spectrosc. **181**, 287 (1997).
[34]T. Shimanouchi, J. Phys. Chem. Ref. Data **1**, 189 (1972).
[35]N. Ohashi, S. Tsunekawa, K. Takagi, and J. T. Hougen, J. Mol. Spectrosc. **137**, 33 (1989).
[36]L. Sztraka, Acta Phys. Hung. **55**, 135 (1984).
[37]J. T. Hougen, I. Kleiner, and M. Godefroid, J. Mol. Spectrosc. **163**, 559 (1994).
[38]N. Ohashi, K. Takagi, J. T. Hougen, W. B. Olson, and W. J. Lafferty, J. Mol. Spectrosc. **132**, 242 (1988).
[39]C. H. Townes and A. L. Schawlow, *Microwave Spectroscopy* (Dover, New York, 1975).
[40]M. A. Mekhtiev, P. D. Godfrey, and J. T. Hougen, J. Mol. Spectrosc. **194**, 171 (1999).
[41]S. M. Lederman, J. H. Runnels, and R. A. Marcus, J. Phys. Chem. **87**, 4364 (1983).
[42]W. D. Lawrance and A. E. W. Knight, J. Phys. Chem. **89**, 917 (1985).
[43]K. K. Lehmann, J. Phys. Chem. **95**, 7556 (1991).
[44]W. D. Lawrance and A. E. W. Knight, J. Phys. Chem. **92**, 5900 (1988).
[45]D. G. Burkhard and D. M. Dennison, J. Mol. Spectrosc. **3**, 299 (1959).
[46]L.-H. Xu and J. T. Hougen, J. Mol. Spectrosc. **173**, 540 (1995).
[47]R. H. Hunt, W. N. Shelton, W. B. Cook, O. N. Bignall, J. W. Mirick, and F. A. Flaherty, J. Mol. Spectrosc. **149**, 252 (1991).
[48]Y.-C. Chou and J. T. Hougen, J. Chem. Phys. **124**, 074319 (2006).
[49]D. S. Perry, J. Mol. Spectrosc. **257**, 1 (2009).